HHS Public Access

Author manuscript

Neurobiol Dis. Author manuscript; available in PMC 2025 May 14.

Published in final edited form as:

Neurobiol Dis. 2025 May ; 208: 106859. doi:10.1016/j.nbd.2025.106859.

Potentiation of the M_1 muscarinic acetylcholine receptor normalizes neuronal activation patterns and improves apnea severity in *Mecp2*$^{+/-}$ mice

Mackenzie Smith[a,b], **Grace E. Dodis**[a,b], **Amanda M. Vanderplow**[a,b], **Sonia Gonzalez**[a,b], **Yewon Rhee**[a,b], **Karie Scrogin**[a,b], **Rocco G. Gogliotti**[a,b,*]

[a] Department of Molecular Pharmacology and Neuroscience, Loyola University Chicago, 2160 S 1st Avenue, Maywood, IL 60153, USA

[b] Edward Hines Jr. VA Hospital, 5000 5th Ave, Hines, IL 60141, USA

Abstract

Rett syndrome (RTT) is a neurodevelopmental disorder that is caused by loss-of-function mutations in the *methyl-CpG binding protein 2* (*MeCP2*) gene. RTT patients experience a myriad of debilitating symptoms, which include respiratory phenotypes that are often associated with lethality. Our previous work established that expression of the M_1 muscarinic acetylcholine receptor (mAchR) is decreased in RTT autopsy samples, and that potentiation of the M_1 receptor improves apneas in a mouse model of RTT; however, the population of neurons driving this rescue is unclear. Loss of Mecp2 correlates with excessive neuronal activity in cardiorespiratory nuclei. Since M_1 is found on cholinergic interneurons, we hypothesized that M_1-potentiating compounds decrease apnea frequency by tempering brainstem hyperactivity. To test this, *Mecp2*$^{+/-}$ and *Mecp2*$^{+/+}$ mice were screened for apneas before and after administration of the M_1 positive allosteric modulator (PAM) VU0453595 (VU595). Brains from the same mice were then imaged for c-Fos, ChAT, and Syto16 using whole-brain light-sheet microscopy to establish genotype and drug-dependent activation patterns that could be correlated with VU595's efficacy on apneas. The vehicle-treated *Mecp2*$^{+/-}$ brain exhibited broad hyperactivity when coupled with the phenotypic prescreen, which was significantly decreased by administration of VU595, particularly in regions known to modulate the activity of respiratory nuclei (i.e. hippocampus and striatum). Further, the extent of apnea rescue in each mouse showed a significant positive correlation with c-Fos expression in non-cholinergic neurons in the striatum, thalamus, dentate gyrus, and within the

* Corresponding author at: Department of Molecular Pharmacology and Neuroscience, Loyola University Chicago, 2160 S. 1st Avenue, Maywood, IL 60153, USA. rgogliotti@luc.edu (R.G. Gogliotti).

Declaration of competing interest

The authors declare that they have no known competing financial interests or personal relationships that could have appeared to influence the work reported in this paper.

CRediT authorship contribution statement

Mackenzie Smith: Writing – review & editing, Writing – original draft, Project administration, Methodology, Investigation, Formal analysis, Conceptualization. **Grace E. Dodis:** Writing – review & editing, Investigation. **Amanda M. Vanderplow:** Writing – review & editing, Investigation. **Sonia Gonzalez:** Writing – review & editing, Investigation. **Yewon Rhee:** Writing – review & editing, Investigation. **Karie Scrogin:** Supervision, Software, Resources, Methodology, Investigation. **Rocco G. Gogliotti:** Writing – review & editing, Supervision, Resources, Methodology, Conceptualization.

Supplementary data to this article can be found online at https://doi.org/10.1016/j.nbd.2025.106859.

cholinergic neurons of the brainstem. These results indicate that *Mecp2*$^{+/-}$ mice are prone to hyperactivity in brain regions that regulate respiration, which can be normalized through M_1 potentiation.

Keywords

Rett syndrome; Apneas; M1 mAchR; Light sheet imaging; C-Fos

1. Introduction

RTT is a neurodevelopmental disorder that is caused by *de novo* mutations in a transcription factor known as *methyl CpG binding protein 2* (*MeCP2*) (Amir et al., 1999; Hagberg, 2002). MeCP2 forms a molecular bridge between methylated DNA and chromatin, and mutations that disrupt either interaction are pathogenic (Amir et al., 1999). Clinically, RTT patients experience a period of normal development, followed by stagnation and then rapid regression between 6 and 18 months of age. During this time, acquired social, motor, and cognitive abilities are lost, and symptoms such as breathing irregularities, seizures, and hand-clasping stereotypies develop. These symptoms never resolve and result in severe disability over the patient's entire life (Feldman et al., 2016; Vashi and Justice, 2019). Current treatment options are limited; however, work from our lab has supported the potential utility of drugs that target the M_1 muscarinic acetylcholine receptor. Specifically, we demonstrated that M_1 expression is decreased in the temporal cortex of 40 RTT autopsy samples and that administration of an M_1 positive allosteric modulator VU0453595 (PAM, VU595) improves social, cognitive, and apnea phenotypes in a *Mecp2*$^{+/-}$ mouse model (Smith et al., 2022).

While the M_1 receptor has a well-defined role in social and cognitive phenotypes (Rusted and Warburton, 1988; Bodick et al., 1997), the mechanisms by which it modifies respiratory patterns are poorly understood. This phenotype is crucial to understand in the context of RTT, where persistent episodes of alternating hyperventilation and breath-holding induce oxidative stress on the autonomic neurons innervating the heart. This pathology is linked to the development of long QT syndrome, which disrupts cardiac rhythm and is responsible for a significant portion of deaths in RTT patients (Bissonnette and Knopp, 2006; Weese-Mayer et al., 2006; Tarquinio et al., 2015; Ramirez et al., 2020; Cordani et al., 2023). The capacity of the M_1 receptor to rescue apneas in RTT is paradoxical, as the receptor is enriched in the forebrain, but has only minimal expression in the brainstem (Miyoshi et al., 1989; Mallios et al., 1995; Lebois et al., 2018). While the function of excitatory, inhibitory, and modulatory neurons are all compromised within the respiratory nuclei of RTT mice, it is unclear what therapies can be used to normalize activity in these circuits (Ward et al., 2020). One important study found that expression of the immediate early gene c-Fos is increased in brain regions responsible for coordinating the respiratory response to stimuli (i.e. the nucleus tractus solitarus (nTs)) in male *Mecp2*$^{-/y}$ models (Kron et al., 2012), indicative of excessive neuronal activity. Chemogenetic activation of pyramidal neurons in the medial prefrontal cortex (mPFC) reduces apneas in RTT via long-range, excitatory projections to the locus coeruleus (LC) and its associated connections with respiratory nuclei (Howell

et al., 2017). The mPFC regulates behavioral state, and these data align with reports that stress can influence apnea severity (Ren et al., 2012). As M_1 is both present in brainstem cholinergic interneurons and enriched in the mPFC, there are several potential mechanisms by which M_1 PAMs correct apneas.

In this study, we combine whole-body plethysmography (WBP) with whole-brain light-sheet imaging to take a non-biased approach to 1) establish genotype-dependent neuronal activation patterns following WBP, 2) identify M_1 PAM-specific drug signatures throughout the brain, and 3) correlate neuronal activity with the degree of apnea rescue conferred by M_1 potentiation. These experiments showed that frontal and cerebellar regions exhibit significant hyperactivity in *Mecp2*$^{+/-}$ mice, which is normalized by VU595 administration. Additionally, the number of c-Fos positive neurons in frontal and midbrain regions positively correlates with the degree of apnea rescue conferred by VU595 in *Mecp2*$^{+/-}$ mice. Lastly, there is a positive correlation between choline acetyltransferase (ChAT) and c-Fos co-staining in the medulla and the degree of apnea rescue induced by VU595 administration. Together, these data demonstrate that the efficacy of M_1 PAMs on respiratory phenotypes is associated with the regulation of non-cholinergic neurons in the fore- and midbrain and cholinergic neurons in the brainstem.

2. Materials and methods

2.1. Animals

Female *Mecp2*$^{+/+}$ and *Mecp2*$^{+/tm1.1\ bird}$ mice were purchased from Jackson Laboratories and maintained until experiments were performed at 20 weeks, the age at which reproducible phenotypes are present in our colony (Gogliotti et al., 2017, 2018; Smith et al., 2022). The model and sex used are in line with the standards of the RTT research community, and only female mice were studied to reflect the overwhelmingly female RTT patient population (Katz et al., 2012). In addition, our sample size of $n = 5$/genotype/treatment for each phase of the experiment is in line with what has previously been used to see a significant effect of genotype on c-Fos expression in mouse models of RTT, or effect of drug in light-sheet imaging experiments (Kron et al., 2012; Davoudian et al., 2023). As Mecp2 mosaicism can impact drug efficacy, a selection criteria was established for the VU595-treated *Mecp2*$^{+/-}$ group requiring apnea rescue of >10 % for inclusion. In this cohort, 5 mice met this criteria and their brains were harvested for light-sheet imaging while 7 had more modest drug effects.

The same n = 5 mice from each group were used for both the WBP and tissue collection phases of the experiment to directly correlate the efficacy of VU595 to reduce apneas with the brain regions activated by drug treatment in each mouse. WBP was first performed on mice from all groups to measure apneas before and after VU595 or vehicle administration, followed 90 min later by collection of whole-brain samples and downstream light-sheet imaging. All experimental procedures were approved and overseen by the Loyola University Chicago Institutional Animal Care and Use Committee.

2.2. Whole body plethysmography (WBP)

Mecp2$^{+/-}$ and *Mecp2*$^{+/+}$ mice (20w) were placed into a WBP chamber (Buxco, FinePointe) and acclimated for 30 min, after which a baseline measure of apneas was recorded for 30 min. Mice were then removed from the chamber and administered 10 mg/kg VU595 in 10 % Tween-80 via intraperitoneal (ip) injection or vehicle (10 % Tween-80 alone) according to their randomly assigned treatment group. We previously established that this dose improves cognitive, social, and respiratory phenotypes in *Mecp2*$^{+/-}$ mice at 30-min post-injection: a timepoint based on the compound's T_{max} (Ghoshal et al., 2016; Smith et al., 2022). Mice were then placed back into WBP chambers, and 30 min post-dose apneas were again measured to establish the degree of rescue in each mouse. Apneas, defined as a breath spanning >1 s, were quantified using FinePointe software.

2.3. Perfusion

In accordance with the methods used in Kron et al., 2012, 90 min post-drug administration, mice were briefly anesthetized with 5 % isoflurane and injected with Euthasol. This was followed by transcardial perfusion with heparinized saline and then 4 % paraformaldehyde (PFA). Whole brains were harvested and post-fixed in 4 % PFA overnight. Samples were stored in PBS + 0.02 % sodium azide before imaging.

2.4. Light sheet imaging

N = 5/genotype/treatment whole mouse brains were processed following the SHIELD protocol (LifeCanvas Technologies, Park et al., 2019). Samples were cleared passively for a week in a delipidation buffer at 45 °C. Cleared samples were then actively immunolabeled using SmartBatch+ (LifeCanvas Technologies) based on eFLASH technology integrating stochastic electrotransport (Kim et al., 2015) and SWITCH (Murray et al., 2015). Each brain sample was stained with primary antibody, 24 µL of Syto16 (Thermo Fisher Scientific Inc., S7578), 40 µL of goat anti-ChAT antibody (MilliporeSigma, AB144P), and 3.5 µg of rabbit c-Fos antibody (Abcam, ab214672) followed by fluorescently conjugated secondaries in 1:2 primary: secondary molar ratio (Jackson ImmunoResearch). After active labeling, samples were incubated in EasyIndex (LifeCanvas Technologies) for refractive index matching (RI = 1.52) and imaged at 3.6× magnification, 1.8 µm/pixel resolution on the XY plane, and 4 µm thickness along the z-axis with a SmartSPIM axially swept light sheet microscope (LifeCanvas Technologies).

Sample images were tile-corrected, destriped, and registered to the Allen Brain Atlas (Allen Institute: https://portal.brain-map.org/) using an automated process. A Syto16 channel for each brain was registered to a custom Syto16-based atlas for the Allen Common Coordinate Framework v3, using successive rigid, affine, and b-spline warping algorithms (SimpleElastix: https://simpleelastix.github.io/). Cell locations were found using a custom semantic segmentation model generated using Tensorflow (https://www.tensorflow.org/). Using the atlas registration, measurements were projected onto the Allen Brain Atlas to quantify the ChAT and c-Fos individual cell counts and ChAT/c-Fos co-expression for each atlas-defined region. Representative 3D images of the brain were made in Imaris, and heat maps were made using the average counts in each group in the program Plotly.

2.5. Statistical analysis

Brain regions that had previously been implicated in regulating RTT-like phenotypes were first selected for analysis (Cerebral cortex and hippocampus = Social and cognitive deficits, striatum and midbrain = cognitive and motor deficits, and hindbrain and brainstem = respiration). Next, more detailed brain regions were selected for analysis by filtering for regions with a depth < 5 in the Basic Cell Groups and Regions of the Allen Brain Atlas. c-fos and ChAT counts were compared between genotype and treatment groups using 2-way ANOVA and Tukey post-hoc tests. Brain regions were omitted from the analysis of ChAT and c-Fos co-positive counts if ChAT was not expressed in that region. Subjects were removed from light-sheet imaging analysis of a brain region if significant damage occurred to that region during sample collection.

Percent apnea increase was calculated using the formula: $\%\ apnea\ increase = \frac{post - drug\ apneas}{baseline\ apneas} \times 100$, and percent apnea rescue was calculated using the formula: $\%\ apnea\ rescue\ = 100 - \left(\frac{post - drug\ apneas}{baseline\ apneas} \times 100\right)$. Correlation analyses were performed using simple linear regression in brain regions implicated in regulating respiration.

2.6. Immunohistochemistry (IHC)

A separate cohort of untreated and minimally handled mice were perfused and used for confirmatory IHC experiments. Free-floating hippocampal sections were cut at 40 μm using a cryostat. Six sections within the hippocampus were selected from each animal, with 240 μm between each section. Samples were washed in PBS, incubated in hydrogen peroxide, and then washed again with PBS before being incubated in 1:1000 rabbit anti-c-Fos antibody (Cell Signaling Technology, 2250) diluted in 0.4 % Triton X-100 for 1 h at room temperature, then for 48 h at 4 °C. After washing, a biotinylated 1:1000 donkey anti-rabbit secondary antibody (Jackson ImmunoResearch Laboratories, 716,065,152) was applied to sections. Elite ABC solution (VectaLabs, PK6100) and DAB Ni (VectaLabs, SK4100) kits were then used to develop the stain according to manufacturer instructions. Sections were mounted, dehydrated, stained with neutral red dye, and cleared with SafeClear. Images were captured with CellSens and c-Fos positive cells were quantified using Photoshop (Adobe, 2021).

3. Results

3.1. c-Fos expression is increased in Mecp2$^{+/-}$ mice and normalized by VU595

Previous work has characterized patterns of hypo- and hyper-activity in the brains of male *Mecp2*$^{-/y}$ mice using c-Fos-stained sections (Kron et al., 2012). Here we used a similar approach coupled to whole-brain light sheet imaging to establish baseline and M_1 PAM activation patterns following a phenotypic prescreen in female *Mecp2*$^{+/-}$ mice. The experimental workflow is outlined in Fig. 1A and was performed on 20-week-old *Mecp2*$^{+/+}$ and *Mecp2*$^{+/-}$ mice. The 20-week timepoint was selected to represent an age where robust phenotypes are reproducibly quantified and responsive to drug treatment within our colony (Gogliotti et al., 2017, 2018; Smith et al., 2022). Control and test mice were 1) habituated to

the whole body plethysmograph for 30 min, 2) measured for baseline apnea numbers, 3) Fig. 2: Brain regions associated with RTT-like phenotypes are hyperactive and normalized by M_1 potentiation in *Mecp2*$^{+/-}$ mice. **A)** Heat maps of average c-Fos counts for each group in a representative section of the brain. **B)** Box plots representing c-Fos positive cells normalized to average *Mecp2*$^{+/+}$ vehicle in brain regions associated with RTT-like phenotypes. N = 4–5/genotype/treatment. Plots span Q1-Q3 with a median centerline. 2-way ANOVA with post-hoc Tukey comparisons test (within each region, compare groups). *$p < 0.05$, **$p <$ 0.01. Subject #130 is excluded from hindbrain and brainstem analysis due to tissue damage.

administered either the M_1 PAM VU595 (ip, 10 mg/kgin 10 % Tween-80) or vehicle (10 % Tween-80), 4) measured for apnea reversal, 5) sacrificed and perfused with PFA, 6) brains were cleared and stained with a nucleic acid marker (Syto 16), a marker of cholinergic neurons (ChAT), and a maker of neuronal activation (c-Fos), 7) whole-brain light sheet microscopy was performed and patterns of pan-neuronal and cholinergic neuronal activation were mapped to all 840 regions of the Allen Brain Atlas. Representative sagittal, transverse, and coronal images for each of the four test groups are shown in Fig. 1B and whole brain 3D videos comparing vehicle-treated *Mecp2*$^{+/+}$ and *Mecp2*$^{+/-}$ mice (#1), and *Mecp2*$^{+/-}$ mice treated with vehicle and VU595 (#2) are provided in Movies 1–2.

We first used this approach to establish genotype and drug-specific activity signatures in *Mecp2*$^{+/-}$ and *Mecp2*$^{+/+}$ mice in all cells marked only by c-Fos, as opposed to c-Fosplus a secondary marker. Relative to vehicle-treated *Mecp2*$^{+/+}$ mice, heat maps showing average c-Fos counts reveal a consistent pattern of increased activity throughout the vehicle-treated *Mecp2*$^{+/-}$ brain, which is reversed by VU595 administration (Fig. 2A). To account for the fact that behavioral state can impact apnea severity, we initially examined a panel of umbrella brain regions implicated in the regulation of several different RTT-like phenotypes (Fig. 2B) (Gabbott et al., 2005; Weese-Mayer et al., 2006; Ren et al., 2012). In this analysis, the number of c-Fos positive neurons in vehicle-treated *Mecp2*$^{+/-}$ mice normalized to *Mecp2*$^{+/+}$ controls had a broad pattern of hyperactivity (green bars), which reached significance in the hippocampus and striatum and was rescued with VU595 administration (purple bars). No significant differences were found between groups in the cerebral cortex, midbrain, hindbrain, and brainstem.

Previously, it was reported that RTT model mice have no difference in hippocampal c-Fos levels at baseline, which contrast the data reported here (Kron et al., 2012). To address the possibility that the hyperactivity we observed in our experiments was due to the stress of the phenotypic prescreen, we generated and processed a new cohort of naive micein the absence of any stimuli or treatment. IHC staining showed that there was no significant difference in hippocampal c-Fos expression between RTT mice and littermate controls absent these stimuli (Fig. 3A–C), strongly suggesting that neuronal hyperactivity observed was a function of the phenotypic prescreen.

To address the possibility that M_1 potentiation could be regulating more granular brain regions, we performed an analysis of all divisions nested under “Basic Cell Groups and Regions” in the Allen Brain Atlas with depth < 5 parent structures in the tree, which amounted to 28 sub regions. Post-hoc comparisons and significant differences between

genotype and/or treatment are listed in Supplemental Table 1, and a comprehensive list of c-Fos activation across the 840 Allen Brain Atlas is provided in Supplemental Table 2. As we anticipated, many of the 28 regions examined showed significant genotype and/or drug effects not represented in the initial umbrella analysis. One example is in the cerebellum, which was not significantly affected when analyzed as an aggregate. With this more focused approach, we quantified a significant increase in c-Fos positive cells in vehicle-treated *Mecp2*$^{+/-}$ mice in three cerebellar nuclei (fastigial, interposed, and dentate nucleus), as well as in the vestibulocerebellar nucleus (Fig. 4). VU595 normalized activity patterns to wild type levels in these regions, indicative of a "cooling" effect on neuronal activity that is more pronounced in some sub-regions relative to others.

3.2. M_1 PAM-mediated c-Fos activation in cholinergic cells is region-specific

The initial analysis of c-Fos staining in unspecified neuronal populations indicated a general inhibitory effect of M_1 potentiation, which aligns with the predicted response from activation of cholinergic interneurons. To determine whether this was the case, we next examined the pattern of ChAT and c-Fos co-staining. Heat maps of these results in each experimental group are provided in Fig. 5A. Similar to the previous analysis, the number of c-Fos and ChAT co-positive neurons normalized to *Mecp2*$^{+/+}$ controls were first analyzed in umbrella brain regions known to regulate RTT-like behaviors (Fig. 5B). In the hippocampus, the number of c-Fos positive cholinergic neurons was significantly increased in VU595-treated control *Mecp2*$^{+/+}$ mice, consistent with known enrichment of the M_1 receptor in that region (Levey et al., 1995).

Three distinct patterns of cholinergic neuronal activation were evident in the comprehensive analysis of 26 "Basic Cell Groups and Regions" examined in the Allen Brain Atlas (fastigial and vestibulocerebellar nuclei were excluded from this analysis due to no ChAT+Fos co-expression in these regions). These patterns showed that 1) many regions do not exhibit significant differences between genotypes or treatment groups, including the cerebrum and brainstem; 2) VU595-treated control *Mecp2*$^{+/+}$ mice have increased ChAT+c-Fos co-positive staining in cortical, midbrain, and cerebellar regions; and 3) vehicle-treated *Mecp2*$^{+/-}$ mice also have increased activity of cholinergic neurons in midbrain and cerebellar regions, which is decreased following administration of VU595 (Fig. 6). When analyzed in concert with the data from staining c-Fos alone, these results point to a broad pattern of hyperactivity in the brains of *Mecp2*$^{+/-}$ mice. Post-hoc comparisons and significant differences between genotype and/or treatment are listed in Supplemental Table 3, and a comprehensive list of c-Fos and ChAT activation across the Allen Brain Atlas is provided in Supplemental Table 4.

3.3. Activity in c-Fos + ChAT neurons correlates with efficacy in reducing apneas

RTT is an X-linked disorder, and female patients and model mice are mosaic for the wild type and mutant alleles. Consequently, the random distribution pattern of the mutant allele can lead to heterogeneity in disease presentation and treatment response. To account for variability, we performed a phenotypic pre-screen of the mice used to generate Figs. 2–6 to establish the percentage of M_1-PAM-dependent apnea reversal within each individual mouse, which could then be correlated with the magnitude of c-Fos activation across their brain. The number of apneas at baseline and following drug treatment is shown in

Fig. 7A–D. In line with our previous findings (Smith et al., 2022), *Mecp2*$^{+/-}$ mice who were administered VU595 showed a significant reduction in apnea number. Conversely, vehicle-treated *Mecp2*$^{+/-}$ mice had significantly more apneas relative to baseline, potentially indicative of increased stress associated with the test.

We initially compared c-Fos expression relative to percent apnea increase (vehicle) or decrease (VU595 in *Mecp2*$^{+/-}$ mice independent of cellular identity. This analysis showed no significant correlations in total gray matter or brain regions containing respiratory nuclei in either group (Fig. 7E–H, brainstem region, medulla, pons). In contrast, we quantified a significant correlation between the number of c-Fos positive neurons activated by VU595 administration and the degree of apnea reversal in brain regions that project to respiratory nuclei, either directly or indirectly. These regions include the thalamus, dentate gyrus, and striatum (Fig. 7 I–L). No significant correlations between apnea increase and c-Fos expression were quantified in vehicle-treated *Mecp2*$^{+/-}$ mice.

We next compared the magnitude of c-Fos activation in ChAT-positive neurons relative to percent apnea increase (vehicle) or decrease (VU595) in *Mecp2*$^{+/-}$ mice. Overall, there was no correlation between apnea increase and cholinergic activity in the vehicle control *Mecp2*$^{+/-}$ group (Fig. 8). In direct contrast to what was observed with c-Fos alone, VU595-treated *Mecp2*$^{+/-}$ mice showed a significant correlation between the percentage of apnea rescue and the number of activated cholinergic neurons in the brainstem and medulla (Fig. 8 A–C), where respiratory nuclei are located. No significant correlation was seen in the pons (Fig. 8D). Again in opposition to c-Fos alone, we did not quantify significant correlations in regions that project to respiratory nuclei (Fig. 8E–G, thalamus, dentate gyrus, and striatum). Interestingly, we observed a significant negative correlation in the hippocampus, where less cholinergic activation was associated with a greater decrease in apneas (Fig. 8H). Together, these data may suggest that M_1 activation in regions outside of respiratory nuclei stimulates cholinergic neurons within the brainstem to enhance inhibitory tone and normalize hyperactivity in *Mecp2*$^{+/-}$ mice.

4. Discussion

Respiratory phenotypes in RTT patients and model mice are state-dependent, where factors like anxiety can impact the severity and prevalence of apneas (Weese-Mayer et al., 2006; Ren et al., 2012). Consistent with this theory, our data demonstrate a pattern of increased expression of the immediate early gene c-Fos in brain regions that contribute to both respiratory and behavior state of *Mecp2*$^{+/-}$ mice that have undergone a phenotypic pre-screen. Our results also show that the activation of non-cholinergic neurons in frontal and midbrain regions and cholinergic neurons of the brainstem correlate with the magnitude of M_1 PAM-dependent apnea rescue in RTT model mice (Fig. 9). These studies provide a blueprint for how drug efficacy can be correlated with neuronal activation patterns in a non-biased manner using whole-brain light sheet imaging.

The theory that decreasing hyperactivity is associated with a normalized apnea phenotype appears contradictory to our finding of a positive correlation between apnea rescue and c-Fos expression (Figs. 2, 3, and 7). A closer examination of the regions and cell types

engaged in VU595-treated *Mecp2*$^{+/-}$ mice explains how these results can be reconciled. Our results suggest that excitatory neurons in frontal regions (Fig. 7 I–K) project to cholinergic neurons in the brainstem (Fig. 8B–C), thereby increasing inhibitory tone on hyperactive respiratory nuclei (Fig. 9). Such a context could explain how M_1 potentiation resolves apneas, given that it is primarily enriched in frontal regions (Lebois et al., 2018). It is paradoxical that increased cholinergic activation correlates with apnea rescue, given that the pattern of hyperactivity is independent of cell type *Mecp2*$^{+/-}$ mice. While speculative, this may indicate that the reduction of excitatory tone and the preservation of cholinergic tone are crucial to improving apneas in RTT. These results could also point to a smaller subset of cholinergic interneurons within the medulla, which regulate respiratory circuits directly (Miyoshi et al., 1989; Mallios et al., 1995). While VU595 treatment maintains selective activation in key circuits, neuronal hyperactivation is substantial and indiscriminate in vehicle-treated *Mecp2*$^{+/-}$ mice. This was demonstrated in Figs. 2 and 3, and in the lack of any correlation between c-fos staining and phenotype in Figs. 7 and 8. Additionally, the average number of c-Fos positive cells across the whole brain in vehicle-treated *Mecp2*$^{+/-}$ animals was nearly 6 million (Supplemental Table 2) while there was only an average of 5 k ChAT and c-Fos co-positive cells (Supplemental Table 4). This leaves a considerable number of yet undefined cell populations which may have contributed to our results. Further work is required to tease apart the mechanistic basis of this correlation and the cell types involved.

In support of our proposed model, one study previously showed that activating excitatory CamKIIa-positive neurons projecting from the PFC to the brainstem can inhibit brainstem hyperactivity in the nTS, a medullar subregion (Howell et al., 2017). As our data indicate the involvement of inhibitory medullar cholinergic neurons in apnea rescue, the same or a similar circuit as described in Howell et al., 2017, may account for our results. Additionally, as the PFC regulates stress response (Frysztak and Neafsey, 1991; Goodman et al., 2022), the results of that study and our own also affirm that respiratory phenotypes in RTT are state-dependent. The importance of behavioral state in apnea severity has been established in both RTT humans and mice, where factors like anxiety can impact the severity and prevalence of apneas (Weese-Mayer et al., 2006; Ren et al., 2012). Our data align with these findings, as we report increased expression of the immediate early gene c-Fos throughout the brain of *Mecp2*$^{+/-}$ mice after a phenotypic pre-screen, which contrasts with published reports from mice harvested at baseline (Kron et al., 2012). It has been shown that respiratory abnormalities are correlated with blood corticosterone levels in RTT mice (Ren et al., 2012), and therefore our findings may more directly correlate with state-dependent respiratory phenotypes as opposed to apneas at rest. This may also explain why vehicle-treated *Mecp2*$^{+/-}$ mice have enhanced apneas relative to their baseline in our studies (Fig. 7C).

Our initial analyses quantified a significant increase in c-Fos positive neurons in the hippocampus and striatum of *Mecp2*$^{+/-}$ mice, which was both rescued by VU595 administration and correlated with a decrease in apneas. The striatum and hippocampus are known to mediate response to stress (Jacobson and Sapolsky, 1991; Plattner et al., 2015), further bolstering the hypothesis that there is a behavioral component in mediating the presence and severity of apneas. The hippocampus has also been directly implicated in mediating respiration via the prefronto-thalamic network (Basha et al., 2023). In this circuit,

respiratory rhythm is relayed through thalamic nuclei, which then act as a bridge between the PFC and hippocampus to promote neuronal synchrony required for the cognitive operations performed by these regions. Lastly, the M_1 receptor is highly enriched in the PFC, hippocampus, and striatum (Weiner et al., 1990; Levey et al., 1991), and the Allen brain atlas indicates that its expression is higher in excitatory neurons that project out of these regions. In this context, a loss of M_1 expression would reduce excitatory drive onto inhibitory neurons, resulting in the hyperactivity reported here and by others (Zhang et al., 2008; Kron et al., 2012). Such a mechanism explains how potentiation of M_1 in peripheral regions could normalize brainstem activity.

The results of the experiments described herein further enhance our understanding of M_1 in RTT. Our previous manuscript demonstrated that M_1 potentiation rescues apneas in addition to social and cognitive behaviors linked to hippocampal regulation (Smith et al., 2022). Further, our bulk RNA and protein analyses in the brainstem of VU595-treated *Mecp2*$^{+/-}$ mice suggest that mediating excitatory signaling is key to the effects of VU595. We found that acute injection of VU595 increased inhibition of the kinase Gsk3β and increased presence of the NR2 NMDA receptor subunit in brainstem synaptosomes (Smith et al., 2022). Unfortunately, the process of clearing brain samples and staining precludes follow-up analyses using methods such as *in situ* hybridization. Therefore, further exploration between VU595 and modulation of this axis in discrete brain regions could not be assessed here but remains a future direction to pursue.

Our experiments largely agree with what is currently known about the excitatory-inhibitory imbalance in RTT, particularly with regard to inhibitory neurotransmission. Removing MeCP2 from inhibitory neurons produces RTT-like phenotypes in mice, which are rescued when MeCP2 levels are restored in this cell type (Chao et al., 2010; Ure et al., 2016). Moreover, enhancing GABAergic signaling improves respiratory phenotypes (Abdala et al., 2010; Johnson et al., 2020; Wu et al., 2021). These findings suggest that a global lack of inhibitory tone plays a role in respiratory dysfunction in RTT. Our results showing that cholinergic activation within the medulla correlates with reduced apneas further support this view.

One unexpected result was that VU595 administration significantly decreased c-Fos expression in the cerebellum of *Mecp2*$^{+/-}$ mice, as this brain region is not commonly implicated in phenotypes rescued by M_1 PAMs. However, altered gene expression, including decreased M_1 receptor levels, has been observed in human post-mortem cerebellar samples from RTT patients (Gogliotti et al., 2018) and our data further suggest a role for M_1 signaling in that brain region. Additionally, projections from the cerebellum target respiratory nuclei such as the Kölliker-Fuse nucleus and locus coeruleus, and activity in the cerebellum is increased during respiratory challenge (Teune et al., 2000; Critchley et al., 2015; Schwarz et al., 2015; Fujita et al., 2020). We also noted significant effects of genotype and treatment on c-Fos and ChAT co-positive staining in the cerebellum, further highlighting the capacity of M_1 to modulate neuronal activity in that region. Together, this provides several routes by which disrupted cerebellar activity in RTT is linked to M_1 activity and respiration.

We acknowledge that the hyperactivity phenotype reported in fore and midbrain structures here is in direct contrast to the hypoactivity phenotype described in these regions by others (Kron et al., 2012). However, several key differences in experimental design could account for this discrepancy. The most critical is likely that historical studies have been performed at a resting baseline, whereas our light-sheet imaging experiments involved handling, injection, and WBP steps that may induce stress. Our IHC experiments confirmed that there are no differences in hippocampal c-Fos expression in the absence of stimuli, as reported previously (Kron et al., 2012). Therefore, the hyperactivity observed in the hippocampus by light-sheet imaging post-whole-body plethysmography screen can be attributed to the stress of handling. MeCP2 is an activity-dependent gene regulator, and it is known that excitatory neurons in regions like the hippocampus maintain a prolonged state of activation following stimulation and are prone to hyperexcitability following a challenge with excitatory stimuli (Zhang et al., 2008; Li et al., 2016). Consequently, the increase in c-Fos may be representative of an inability of activated neurons to reset patterns of immediate early gene expression. A second important variable is that the 20-week-old *Mecp2*$^{+/-}$ mice used in our experiments were older than those in previous reports, which used 6-week-old males and 11-week-old females (Kron et al., 2012). This indicates that the landscape of inhibitory and excitatory disruptions may change with age and disease progression. Continued work in this area will be critical to determining the extent to which these and other variables contribute to the results presented herein.

One limitation of this study is that following random-x-inactivation, the *Mecp2*$^{+/-}$ model we used is mosaic for mutant and wild-type cells, and we could not distinguish effects in each population. While restrictive, this model mimics the realities of the majority of RTT patients, which are female. Therefore, our experiments offer a translationally relevant picture of apnea regulation in RTT brains. Our IHC experiments were also limited in scope. The hippocampus was chosen for confirmatory analysis because of work done by others showing no effect of Mecp2 deletion on c-Fos expression in this region (Kron et al., 2012). These data contrasts with our findings in Fig. 2, and were confirmed to be linked to handling stress in Fig. 3. While the striatum also displayed significantly increased neuron activity in *Mecp2*$^{+/-}$ mice in the light-sheet experiments (Fig. 2), baseline c-Fos expression in this region has not been investigated by others. For this reason, we did not proceed with confirmatory analysis in the striatum.

Currently, there is only one FDA-approved drug for RTT, and our results have implications for future avenues for the development of therapeutics for this disorder. Pharmacological activation of the cholinergic system has previously shown efficacy in clinical trials for schizophrenia and Alzheimer's disease in treating social and cognitive deficits, which are two symptom domains that are also disrupted by mutations in MeCP2 (Bodick et al., 1997; Sauder et al., 2022). This research suggests the potential for repurposing these medications for RTT, including the recently approved xanomeline–trospium formulation, KarXT (Cobenfy) (Kingwell, 2024). Here, we also introduce a methodology for establishing drug and genotype signatures in whole-brain samples, with broad applicability in neuropharmacology. This approach can be used to provide a non-biased view of region-specific effects of therapeutics to help determine the population of cells driving the rescue of a phenotype, or even identify the involvement of unexpected circuits or regions. By

employing this method to characterize the action of the M_1 PAM VU595 in the brain, we show that potentiation of the M_1 receptor corrects hyperactivity in RTT. Further, the effect of M_1 potentiation on apneas is driven by the regulation of activity in both non-cholinergic projections and cholinergic neurons of the brainstem. These results advocate for the use of M_1 PAMs as well as other compounds that temper excitability in the brain as possible treatments for RTT.

Supplementary Material

Refer to Web version on PubMed Central for supplementary material.

Acknowledgments

The authors acknowledge and thank Dr. Gwendolyn Kartje and Dr. Brian Powers for technical instruction and resource sharing. The authors would also like to thank Dr. Colleen Niswender for her intellectual contributions to project planning and manuscript preparation.

Funding

This manuscript was supported by the National Institutes of Health (R01 MH124671 and R21 HD111864), and the International Rett Syndrome Foundation (IRSF 3903) to RGG, and the Arthur J. Schmitt Foundation Leadership Fellow Award to Mackenzie Smith.

Data availability

Data will be made available on request.

References

Abdala APL, Dutschmann M, Bissonnette JM, Paton JFR, 2010. Correction of respiratory disorders in a mouse model of Rett syndrome. Proc. Natl. Acad. Sci. USA 107, 18208–18213. [PubMed: 20921395]

Amir RE, Van den Veyver IB, Wan M, Tran CQ, Francke U, Zoghbi HY, 1999. Rett syndrome is caused by mutations in X-linked MECP2, encoding methyl-CpG-binding protein 2. Nat. Genet. 23, 185–188. [PubMed: 10508514]

Basha D, Chauvette S, Sheroziya M, Timofeev I, 2023. Respiration organizes gamma synchrony in the prefronto-thalamic network. Sci. Rep. 13, 8529. [PubMed: 37237017]

Bissonnette JM, Knopp SJ, 2006. Separate respiratory phenotypes in methyl-CpG-binding protein 2 (Mecp2) deficient mice. Pediatr. Res. 59, 513–518. [PubMed: 16549521]

Bodick NC, Offen WW, Levey AI, Cutler NR, Gauthier SG, Satlin A, Shannon HE, Tollefson GD, Rasmussen K, Bymaster FP, Hurley DJ, Potter WZ, Paul SM, 1997. Effects of Xanomeline, a selective muscarinic receptor agonist, on cognitive function and behavioral symptoms in Alzheimer disease. Arch. Neurol. 54, 465–473. [PubMed: 9109749]

Chao H-T, Chen H, Samaco RC, Xue M, Chahrour M, Yoo J, Neul JL, Gong S, Lu H-C, Heintz N, Ekker M, Rubenstein JLR, Noebels JL, Rosenmund C, Zoghbi HY, 2010. Dysfunction in GABA signalling mediates autism-like stereotypies and Rett syndrome phenotypes. Nature 468, 263–269. [PubMed: 21068835]

Cordani R, Tobaldini E, Rodrigues GD, Giambersio D, Veneruso M, Chiarella L, Disma N, De Grandis E, Toschi-Dias E, Furlan L, Carandina A, Prato G, Nobili L, Montano N, 2023. Cardiac autonomic control in Rett syndrome: insights from heart rate variability analysis. Front. Neurosci. 17, 1048278. [PubMed: 37021139]

Critchley HD, Nicotra A, Chiesa PA, Nagai Y, Gray MA, Minati L, Bernardi L, 2015. Slow breathing and hypoxic challenge: cardiorespiratory consequences and their central neural substrates. PLoS One 10, e0127082. [PubMed: 25973923]

Davoudian PA, Shao L-X, Kwan AC, 2023. Shared and distinct brain regions targeted for immediate early gene expression by ketamine and psilocybin. ACS Chem. Neurosci. 14, 468–480. [PubMed: 36630309]

Feldman D, Banerjee A, Sur M, 2016. Developmental dynamics of Rett syndrome. Neural. Plast. 2016, 1–9.

Frysztak RJ, Neafsey EJ, 1991. The Effect of Medial Frontal Cortex Lesions on Respiration, "Freezing," and Ultrasonic Vocalizations during Conditioned Emotional Responses in Rats. Cereb. Cortex 1, 418–425. [PubMed: 1822749]

Fujita H, Kodama T, Du Lac S, 2020. Modular output circuits of the fastigial nucleus for diverse motor and nonmotor functions of the cerebellar vermis. eLife 9, e58613. [PubMed: 32639229]

Gabbott PLA, Warner TA, Jays PRL, Salway P, Busby SJ, 2005. Prefrontal cortex in the rat: projections to subcortical autonomic, motor, and limbic centers. J. Comp. Neurol. 492, 145–177. [PubMed: 16196030]

Ghoshal A, Rook JM, Dickerson JW, Roop GN, Morrison RD, Jalan-Sakrikar N, Lamsal A, Noetzel MJ, Poslusney MS, Wood MR, Melancon BJ, Stauffer SR, Xiang Z, Daniels JS, Niswender CM, Jones CK, Lindsley CW, Conn PJ, 2016. Potentiation of M1 muscarinic receptor reverses plasticity deficits and negative and cognitive symptoms in a schizophrenia mouse model. Neuropsychopharmacol 41, 598–610.

Gogliotti RG, Senter RK, Fisher NM, Adams J, Zamorano R, Walker AG, Blobaum AL, Engers DW, Hopkins CR, Daniels JS, Jones CK, Lindsley CW, Xiang Z, Conn PJ, Niswender CM, 2017. mGlu $_7$ potentiation rescues cognitive, social, and respiratory phenotypes in a mouse model of Rett syndrome. Sci. Transl. Med. 9, eaai7459. [PubMed: 28814546]

Gogliotti RG, Fisher NM, Stansley BJ, Jones CK, Lindsley CW, Conn PJ, Niswender CM, 2018. Total RNA sequencing of Rett syndrome autopsy samples identifies the M $_4$ muscarinic receptor as a novel therapeutic target. J. Pharmacol. Exp. Ther. 365, 291–300. [PubMed: 29523700]

Goodman AM, Wheelock MD, Harnett NG, Davis ES, Mrug S, Deshpande G, Knight DC, 2022. Stress-induced changes in effective connectivity during regulation of the emotional response to threat. Brain Connect. 12, 629–638. [PubMed: 34541896]

Hagberg B, 2002. Clinical manifestations and stages of rett syndrome. Ment. Retard. Dev. Disabil. Res. Rev. 8, 61–65. [PubMed: 12112728]

Howell CJ, Sceniak MP, Lang M, Krakowiecki W, Abouelsoud FE, Lad SU, Yu H, Katz DM, 2017. Activation of the Medial Prefrontal Cortex Reverses Cognitive and Respiratory Symptoms in a Mouse Model of Rett Syndrome. eNeuro 4: ENEURO.0277–17.2017. [PubMed: 29333487]

Jacobson L, Sapolsky R, 1991. The role of the Hippocampus in feedback regulation of the hypothalamic-pituitary-adrenocortical Axis*. Endocr. Rev. 12, 118–134. [PubMed: 2070776]

Johnson CM, Cui N, Xing H, Wu Y, Jiang C, 2020. The antitussive cloperastine improves breathing abnormalities in a Rett syndrome mouse model by blocking presynaptic GIRK channels and enhancing GABA release. Neuropharmacology 176, 108214. [PubMed: 32622786]

Katz DM, et al. , 2012. Preclinical research in Rett syndrome: setting the foundation for translational success. Dis. Model. Mech. 5, 733–745. [PubMed: 23115203]

Kim S-Y, Cho JH, Murray E, Bakh N, Choi H, Ohn K, Ruelas L, Hubbert A, McCue M, Vassallo SL, Keller PJ, Chung K, 2015. Stochastic electrotransport selectively enhances the transport of highly electromobile molecules. Proc. Natl. Acad. Sci. USA 112. Available at: 10.1073/pnas.1510133112 [Accessed September 1, 2023].

Kingwell K, 2024. FDA approves first schizophrenia drug with new mechanism of action since 1950s. Nat. Rev. Drug Discov. 23, 803. [PubMed: 39333712]

Kron M, Howell CJ, Adams IT, Ransbottom M, Christian D, Ogier M, Katz DM, 2012. Brain activity mapping in *Mecp2* mutant mice reveals functional deficits in forebrain circuits, including key nodes in the default mode network, that are reversed with ketamine treatment. J. Neurosci. 32, 13860–13872. [PubMed: 23035095]

Lebois EP, Thorn C, Edgerton JR, Popiolek M, Xi S, 2018. Muscarinic receptor subtype distribution in the central nervous system and relevance to aging and Alzheimer's disease. Neuropharmacology 136, 362–373. [PubMed: 29138080]

Levey A, Kitt C, Simonds W, Price D, Brann M, 1991. Identification and localization of muscarinic acetylcholine receptor proteins in brain with subtype-specific antibodies. J. Neurosci. 11, 3218–3226. [PubMed: 1941081]

Levey A, Edmunds S, Koliatsos V, Wiley R, Heilman C, 1995. Expression of m1-m4 muscarinic acetylcholine receptor proteins in rat hippocampus and regulation by cholinergic innervation. J. Neurosci. 15, 4077–4092. [PubMed: 7751967]

Li W, Xu X, Pozzo-Miller L (2016) Excitatory synapses are stronger in the hippocampus of Rett syndrome mice due to altered synaptic trafficking of AMPA-type glutamate receptors. Proc Natl Acad Sci USA 113 Available at: 10.1073/pnas.1517244113 [Accessed December 20, 2023].

Mallios VJ, Lydic R, Baghdoyan HA, 1995. Muscarinic receptor subtypes are differentially distributed across brain stem respiratory nuclei. Am. J. Phys. Lung Cell. Mol. Phys. 268, L941–L949.

Miyoshi R, Kito S, Shimoyama M, 1989. Quantitative autoradiographic localization of the M1 and M2 subtypes of muscarinic acetylcholine receptors in the monkey brain. Jpn. J. Pharmacol. 51, 247–256. [PubMed: 2593382]

Murray E, Cho JH, Goodwin D, Ku T, Swaney J, Kim S-Y, Choi H, Park Y-G, Park J-Y, Hubbert A, McCue M, Vassallo S, Bakh N, Frosch MP, Wedeen VJ, Seung HS, Chung K, 2015. Simple, scalable proteomic imaging for high-dimensional profiling of intact systems. Cell 163, 1500–1514. [PubMed: 26638076]

Park Y-G, et al. , 2019. Protection of tissue physicochemical properties using polyfunctional crosslinkers. Nat. Biotechnol. 37, 73–83.

Plattner F, Hayashi K, Hernandez A, Benavides DR, Tassin TC, Tan C, Day J,´ Fina MW, Yuen EY, Yan Z, Goldberg MS, Nairn AC, Greengard, Nestler, Taussig R, Nishi A, Houslay MD, Bibb JA, 2015. The role of ventral striatal cAMP signaling in stress-induced behaviors. Nat. Neurosci. 18, 1094–1100. [PubMed: 26192746]

Ramirez J-M, Karlen-Amarante M, Wang J-DJ, Bush NE, Carroll MS, Weese-Mayer DE, Huff A, 2020. The pathophysiology of Rett syndrome with a focus on breathing dysfunctions. Physiology (Bethesda) 35, 375–390. [PubMed: 33052774]

Ren J, Ding X, Funk GD, Greer JJ, 2012. Anxiety-related mechanisms of respiratory dysfunction in a mouse model of Rett syndrome. J. Neurosci. 32, 17230–17240. [PubMed: 23197715]

Rusted JM, Warburton DM, 1988. The effects of scopolamine on working memory in healthy young volunteers. Psychopharmacology 96. Available at: 10.1007/BF00177553 [Accessed March 21, 2024].

Sauder C, Allen LA, Baker E, Miller AC, Paul SM, Brannan SK, 2022. Effectiveness of KarXT (xanomeline-trospium) for cognitive impairment in schizophrenia: post hoc analyses from a randomised, double-blind, placebo-controlled phase 2 study. Transl. Psychiatry 12, 491. [PubMed: 36414626]

Schwarz LA, Miyamichi K, Gao XJ, Beier KT, Weissbourd B, DeLoach KE, Ren J, Ibanes S, Malenka RC, Kremer EJ, Luo L, 2015. Viral-genetic tracing of the input–output organization of a central noradrenaline circuit. Nature 524, 88–92. [PubMed: 26131933]

Smith M, Arthur B, Cikowski J, Holt C, Gonzalez S, Fisher NM, Vermudez SAD, Lindsley CW, Niswender CM, Gogliotti RG, 2022. Clinical and preclinical evidence for M1 muscarinic acetylcholine receptor potentiation as a therapeutic approach for Rett syndrome. Neurotherapeutics 19, 1340–1352. [PubMed: 35670902]

Tarquinio DC, Hou W, Neul JL, Kaufmann WE, Glaze DG, Motil KJ, Skinner SA, Lee H-S, Percy AK, 2015. The changing face of survival in Rett syndrome and MECP2-related disorders. Pediatr. Neurol. 53, 402–411. [PubMed: 26278631]

Teune TM, Van Der Burg J, Van Der Moer J, Voogd J, Ruigrok TJH, 2000. Topography of cerebellar nuclear projections to the brain stem in the rat. In: Progress in Brain Research. Elsevier, pp. 141–172. Available at: https://linkinghub.elsevier.com/retrieve/pii/S0079612300240144 [Accessed October 24, 2023].

Ure K, Lu H, Wang W, Ito-Ishida A, Wu Z, He L, Sztainberg Y, Chen W, Tang J, Zoghbi HY, 2016. Restoration of Mecp2 expression in GABAergic neurons is sufficient to rescue multiple disease features in a mouse model of Rett syndrome. eLife 5, e14198. [PubMed: 27328321]

Vashi N, Justice MJ, 2019. Treating Rett syndrome: from mouse models to human therapies. Mamm. Genome 30, 90–110. [PubMed: 30820643]

Ward CS, Huang T-W, Herrera JA, Samaco RC, McGraw CM, Parra DE, Arvide EM, Ito-Ishida A, Meng X, Ure K, Zoghbi HY, Neul JL, 2020. Loss of MeCP2 function across several neuronal populations impairs breathing response to acute hypoxia. Front. Neurol. 11, 593554. [PubMed: 33193060]

Weese-Mayer DE, Lieske SP, Boothby CM, Kenny AS, Bennett HL, Silvestri JM, Ramirez J-M, 2006. Autonomic nervous system dysregulation: breathing and heart rate perturbation during wakefulness in young girls with Rett syndrome. Pediatr. Res. 60, 443–449. [PubMed: 16940240]

Weiner DM, Levey AI, Brann MR, 1990. Expression of muscarinic acetylcholine and dopamine receptor mRNAs in rat basal ganglia. Proc. Natl. Acad. Sci. USA 87, 7050–7054. [PubMed: 2402490]

Wu Y, Cui N, Xing H, Zhong W, Arrowood C, Johnson CM, Jiang C, 2021. In vivo evidence for the cellular basis of central hypoventilation of Rett syndrome and pharmacological correction in the rat model. J. Cell. Physiol. 236, 8082–8098. [PubMed: 34077559]

Zhang L, He J, Jugloff DGM, Eubanks JH, 2008. The MeCP2-null mouse hippocampus displays altered basal inhibitory rhythms and is prone to hyperexcitability. Hippocampus 18, 294–309. [PubMed: 18058824]

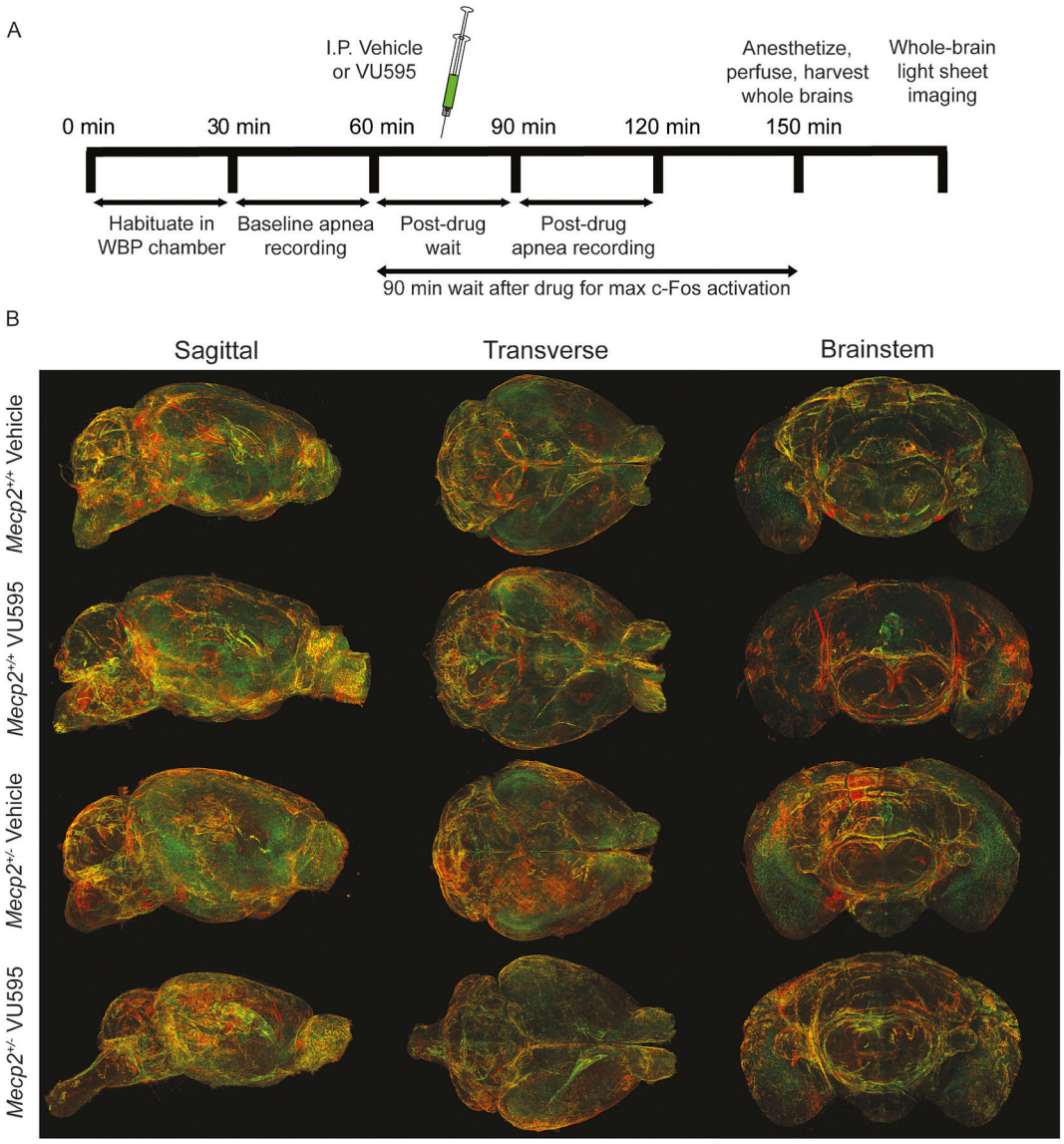

Fig. 1.

Experimental design and representative images. **A)** Schematic of the protocol used prior to whole brain light sheet imaging. A prescreen was performed to measure apneas in *Mecp2*$^{+/+}$ and *Mepc2*$^{+/-}$ mice at baseline and after administration of vehicle (10 % tween-80) or 10 mg/kg VU595. Mice were perfused with PFA 90 min after drug administration and whole brains were harvested and post-fixed to prepare for imaging. **B)** Representative whole-brain light sheet sagittal, transverse, and brainstem images. Red = ChAT; Green = c-Fos.

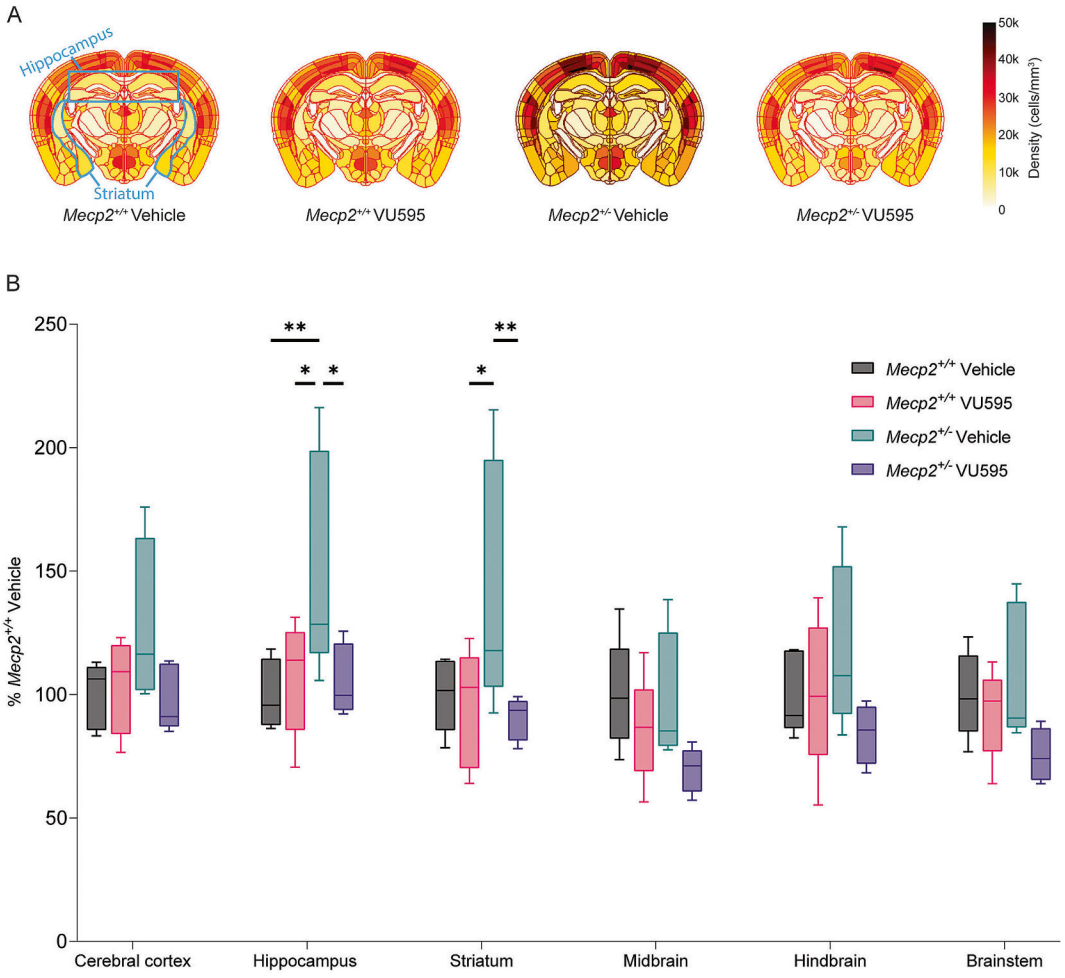

Fig. 2.

Brain regions associated with RTT-like phenotypes are hyperactive and normalized by M_1 potentiation in *Mecp2*$^{+/-}$ mice. **A)** Heat maps of average c-Fos counts for each group in a representative section of the brain. **B)** Box plots representing c-Fos positive cells normalized to average *Mecp2*$^{+/+}$ vehicle in brain regions associated with RTT-like phenotypes. N = 4–5/genotype/treatment. Plots span Q1-Q3 with a median centerline. 2-way ANOVA with post-hoc Tukey comparisons test (within each region, compare groups). *$p < 0.05$, **$p <$ 0.01. Subject #130 is excluded from hindbrain and brainstem analysis due to tissue damage.

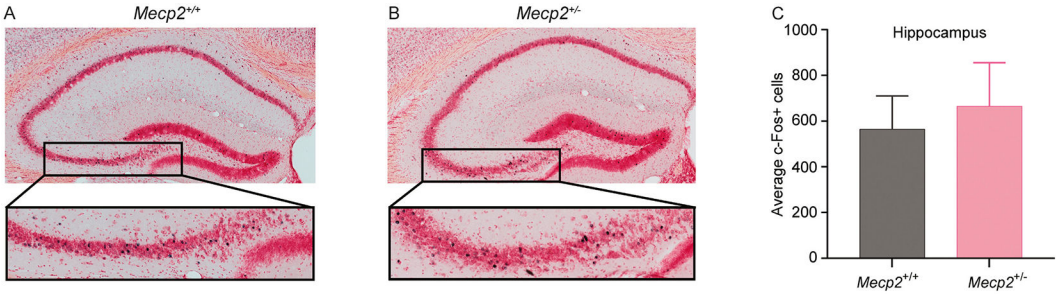

Fig. 3.

Hippocampal c-Fos expression does not differ between *Mecp2*$^{+/+}$ and *Mepc2*$^{+/-}$ mice at baseline: **A-B)** Representative images of **A)** *Mecp2*$^{+/+}$ and **B)** *Mecp2*$^{+/-}$ hippocampus. C-Fos positive cells are indicated by black dots. **C)** Average c-Fos positive cells across 6 sections per animal in *Mecp2*$^{+/+}$ and *Mepc2*$^{+/-}$ samples. $N = 5$/genotype. Data shown represent mean ± SEM. Unpaired *t*-test.

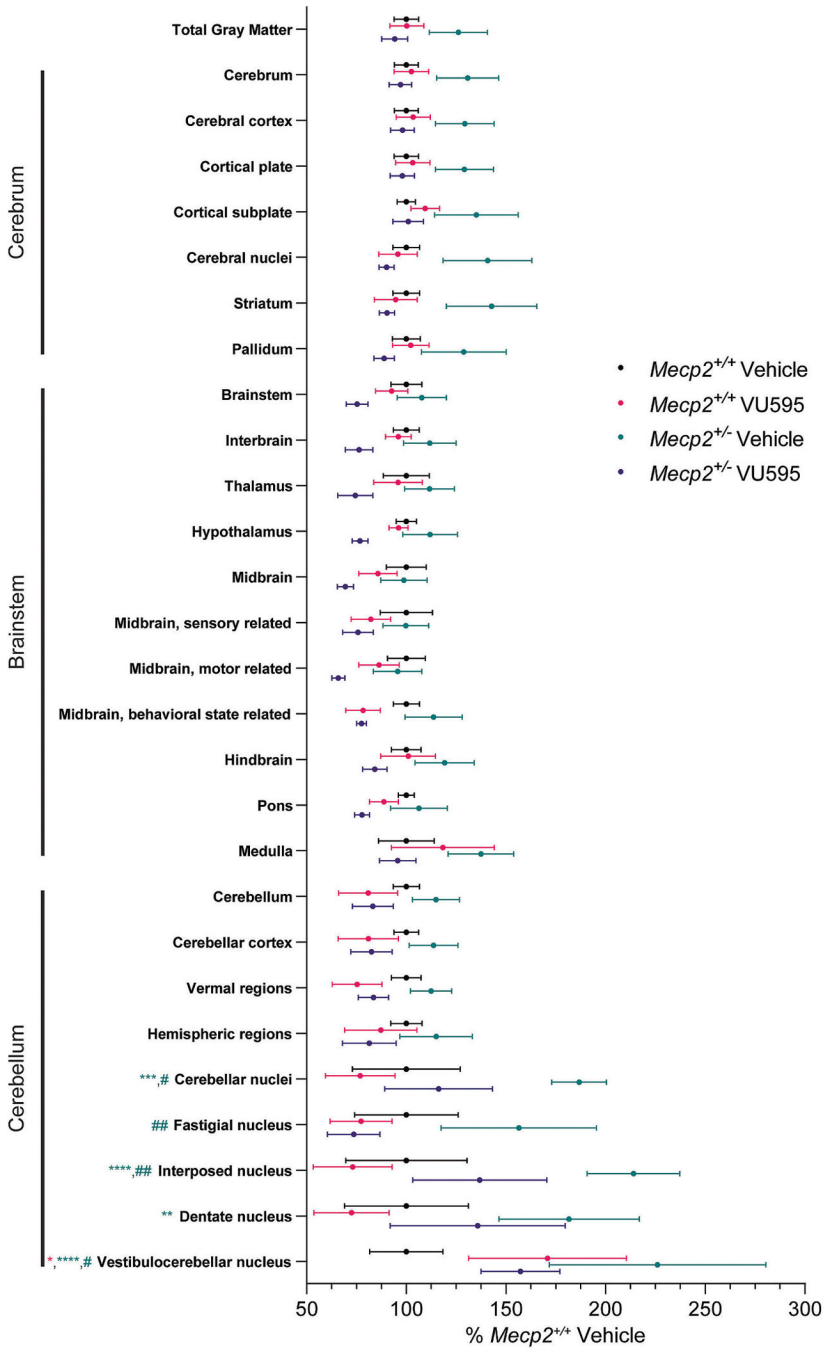

Fig. 4.

Whole brain effects of VU595 on c-Fos expression. Significant increases in c-Fos expression in *Mecp2*$^{+/-}$ mice are seen throughout the brain and normalized by administration of the M_1 PAM VU595. Basic cell groups and regions with a depth < 5 subregions in the Allen Brain Atlas. N = 4–5/genotype/treatment. Data shown represent mean ± SEM. 2-way ANOVA with post-hoc Tukey comparisons test. ***$p < 0.001$, ****$p < 0.0001$ relative to vehicle-treated *Mecp2*$^{+/+}$ mice, #p < 0.05, ##p < 0.01 within genotype comparison. Symbol color

denotes the group showing significant differences. A comprehensive list of statistics and significant comparisons is provided in Supplemental Table 1.

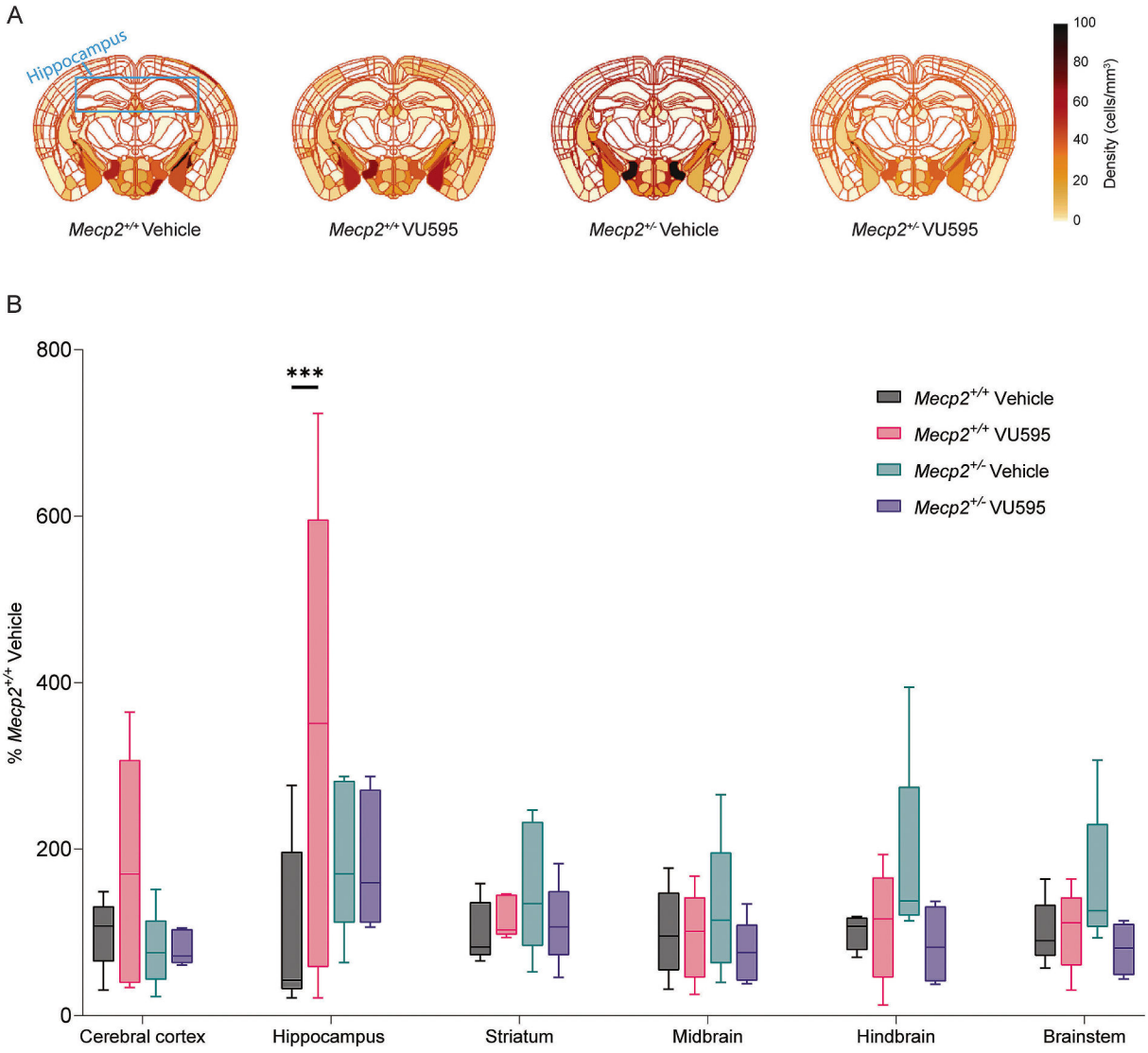

Fig. 5.

Cholinergic neurons in the hippocampus are activated in *Mecp2*$^{+/+}$ mice administered VU595. **A)** Heat maps showing average c-Fos and ChAT co-positive counts for each group in a representative brain section. **B)** c-Fos + ChAT counts normalized to average *Mecp2*$^{+/+}$ vehicle-treated groups in brain regions associated with RTT-like phenotypes. N = 4–5/genotype/treatment. Plots span Q1-Q3 with a median centerline. 2-way ANOVA with post-hoc Tukey comparisons test. ***$p < 0.001$ relative to vehicle-treated Mecp2$^{+/+}$ mice. Subject #130 is excluded from hindbrain and brainstem analysis due to tissue damage.

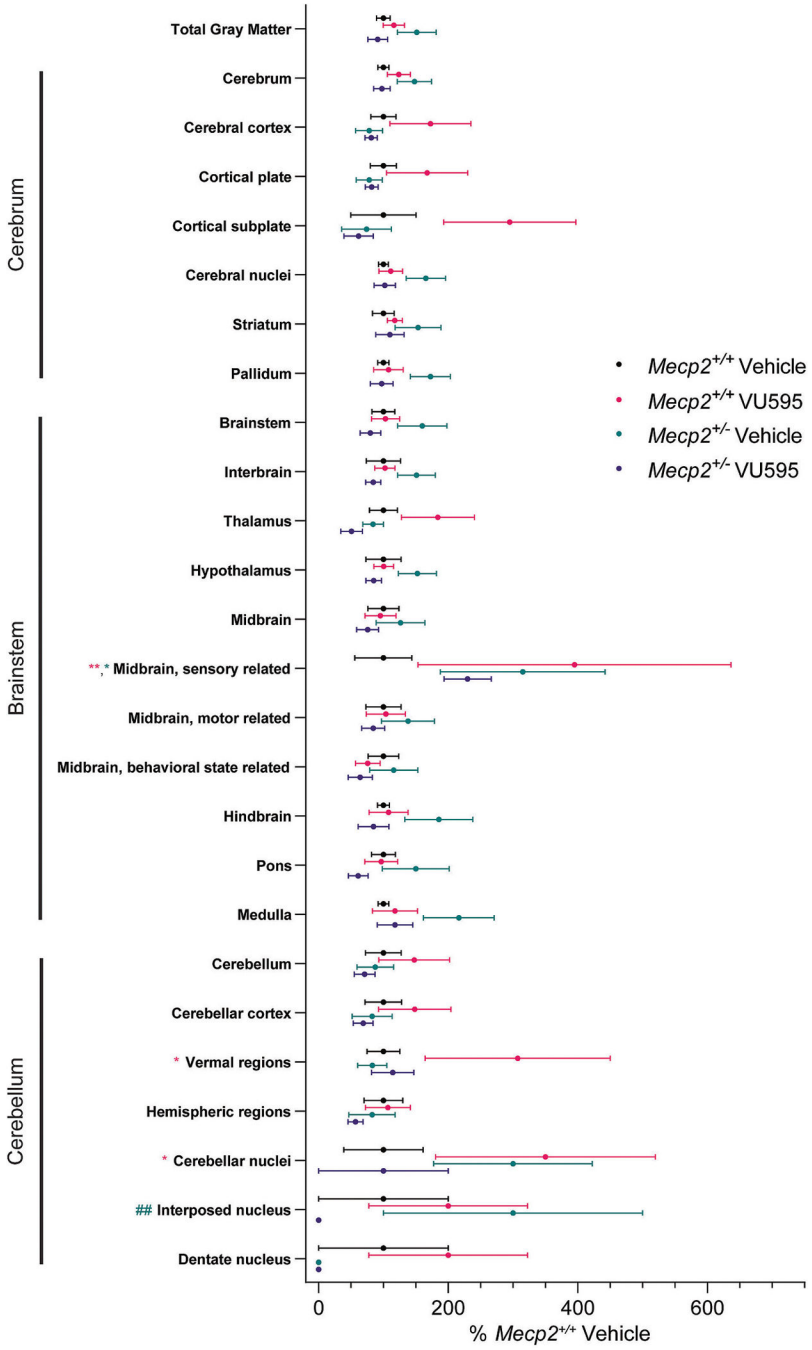

Fig. 6.

Whole brain effects of VU595 on activation of ChAT positive neurons. *Mecp2*$^{+/+}$ and *Mecp2*$^{+/-}$ mice present with region specific genotype and drug effects on ChAT positive neuronal activation. Basic cell groups and regions with a depth < 5 of the Allen Brain Atlas. N = 4–5/genotype/treatment. Data shown represent mean ± SEM. 2-way ANOVA with post-hoc Tukey comparisons test. *p < 0.05, **p < 0.01, relative to vehicle-treated *Mecp2*$^{+/+}$ mice, ##p < 0.01 within genotype comparison. Symbol color denotes the significantly

different group. A comprehensive list of statistics and significant comparisons is provided in Supplemental Table 3.

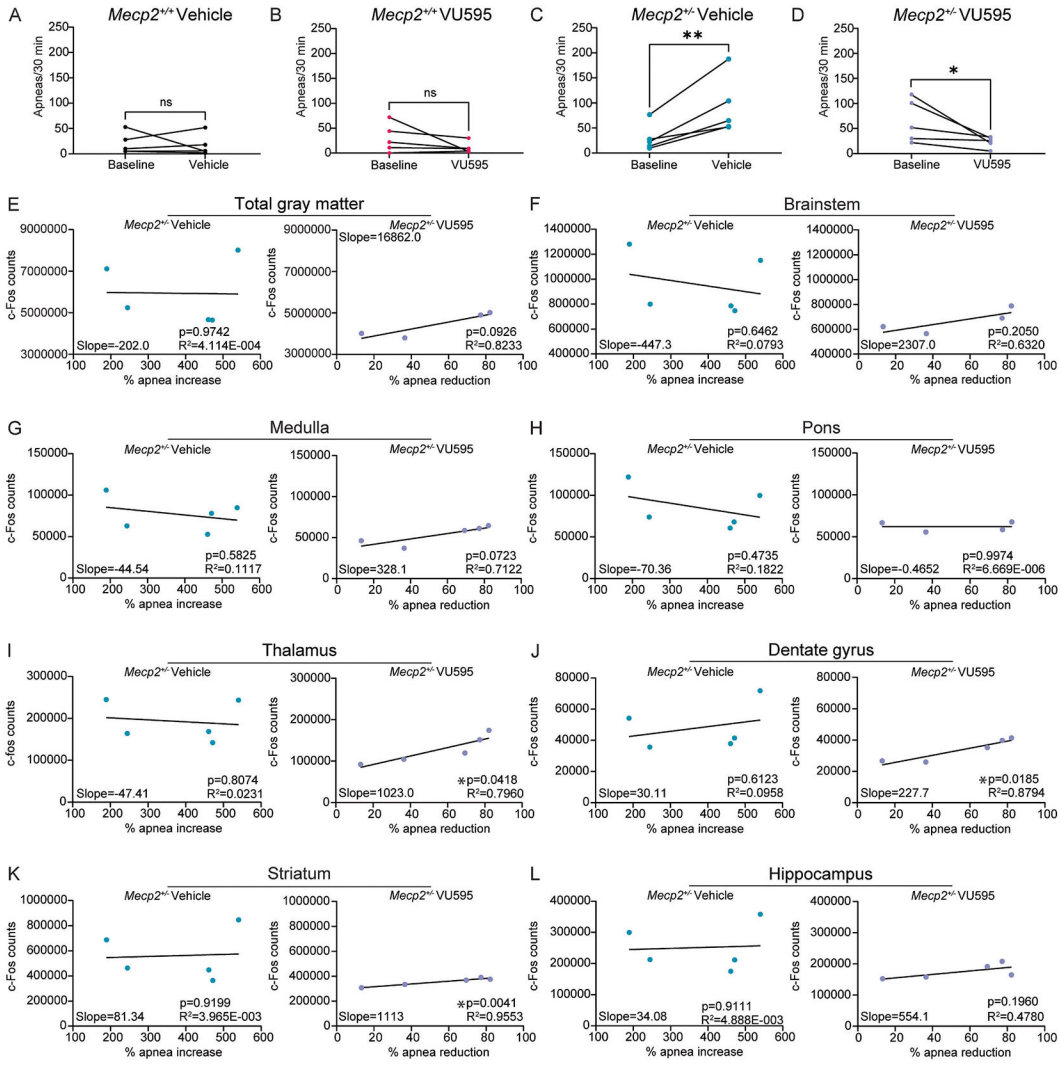

Fig. 7.

The activity of fore- and midbrain neurons is involved in regulating apneas. **A-D)** Whole body plethysmography. N = 5/genotype/treatment. Student's t-test. **A-B)** The respiratory pattern of control *Mecp2*$^{+/+}$ mice is unaffected by vehicle and/or VU595 treatment. **C)** Apneas are significantly increased in vehicle-treated *Mecp2*$^{+/-}$ mice relative to baseline recording. **D)** Consistent with our previous reports, apneas were significantly reduced in *Mecp2*$^{+/-}$ mice following administration of VU595. ***E*-L)** Correlation between c-Fos positive cell counts and % apnea reduction relative to baseline in vehicle- (left) or VU595- (right) treated *Mecp2*$^{+/-}$ mice. Significant correlations were quantified in the thalamus, dentate gyrus, and striatum in the VU595-treated group. N = 4–5/genotype/treatment. Simple linear regression. Subject #130 is excluded from the total gray matter, brainstem, and pons due to significant damage in these regions.

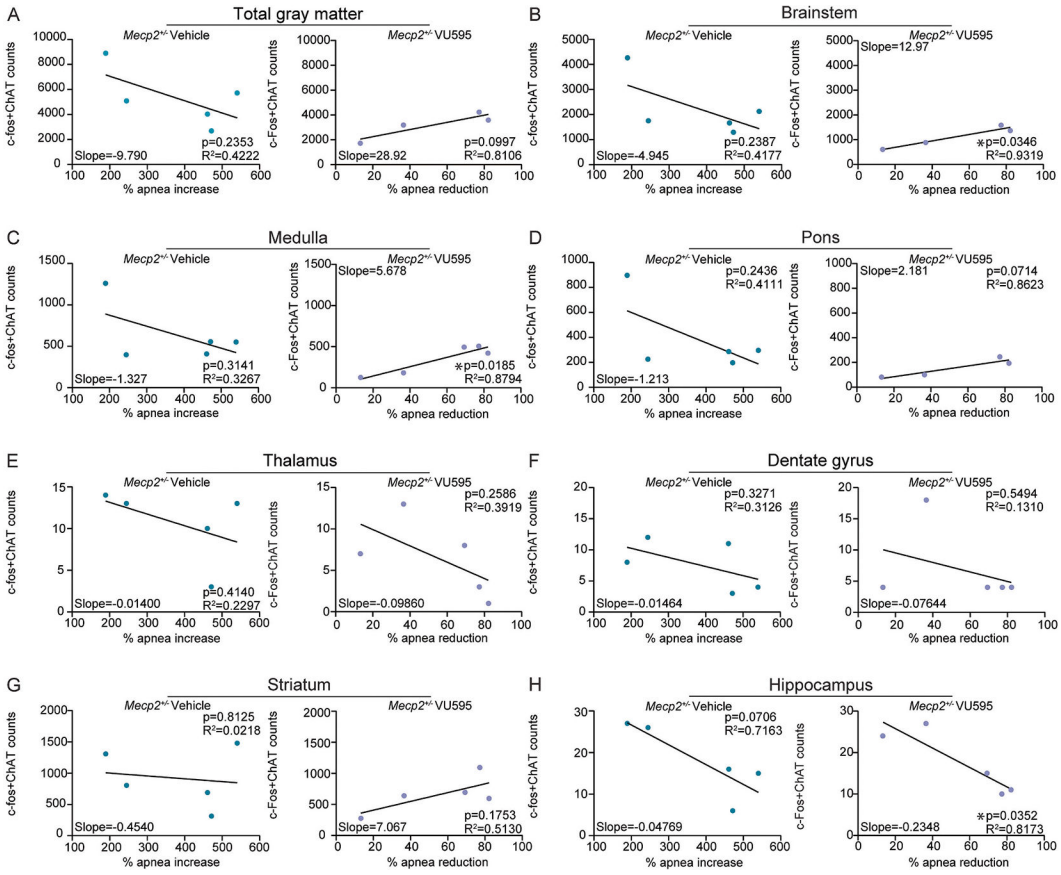

Fig. 8.

The activity of brainstem cholinergic neurons correlates with apnea rescue. N = 4–5/genotype/treatment. **A-H)** Correlation between c-Fos and ChAT co-positive cell counts and % apnea reduction relative to baseline in vehicle- (left) or VU595 (right)-treated *Mecp2*$^{+/-}$ mice. Significant correlations are seen in the brainstem, medulla, and hippocampus (hippocampal region) in the VU595-treated group. Linear regression analysis. Subject #130 is excluded from the total gray matter, brainstem, and pons due to significant damage in these regions. N = 4–5/genotype/treatment.

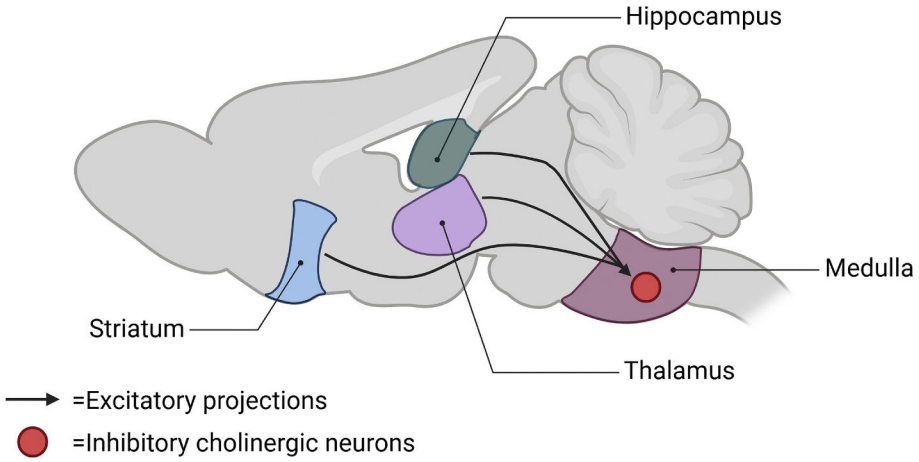

Fig. 9.

Proposed model. Excitatory projections from frontal and midbrain regions either directly or indirectly activate inhibitory cholinergic neurons in the brainstem, leading to the normalization of hyperactivity observed in *Mecp2*$^{+/-}$ mice. Created in BioRender. Gogliotti, R. (2025) https://BioRender.com/y03m797